Submitted to ADVANCED FUNCTIONAL MATERIALS

DOI: 10.1002/adfm.200900801

Photophysics and photocurrent generation in polythiophene/polyfluorene co-polymer blends**

By *Christopher R. McNeill*,* *Agnese Abrusci*, *Inchan Hwang*, *Matthias A. Ruderer*, *Peter Müller-Buschbaum* and *Neil C. Greenham*

[*] Dr. C. R. McNeill, A. Abrusci, I. Hwang, Prof. N. C. Greenham
Cavendish Laboratory, Department of Physics, University of Cambridge, J J Thomson Ave, Cambridge, CB3 0HE, United Kingdom
E-mail: crm51@cam.ac.uk
M. A. Ruderer, Prof. Dr. P. Müller-Buschbaum
Technische Universität München, Physik-Department LS E13, James-Franck-Str. 1, 85747 Garching, Germany

[**] This work was supported by the Engineering and Physical Sciences Research Council, U.K. (SUPERGEN IV). C. R. M. acknowledges the EPSRC for the provision of an Advanced Research Fellowship. I. H. acknowledges the Cavendish-KAIST Research Cooperation Centre for funding. M. A. R. acknowledges the Bavarian State Ministry of Science, Research and Arts for funding through the International Graduate School „Materials Science of Complex Interfaces“ (CompInt). The authors thank Cambridge Display Technology for supplying F8TBT and Henry Snaith (U. Oxford) for helpful discussion. M. A. R. and P. M.-B. thank E. Metwalli, V. Körstgens and R. Meier for assistance with the GISAXS measurements. Supporting Information is available online from Wiley InterScience or from the author.

Abstract:

We have studied the evolution of photophysics and device performance with annealing of blends of poly(3-hexylthiophene) with the two polyfluorene co-polymers poly((9,9-dioctylfluorene)-2,7-diyl-alt-[4,7-bis(3-hexylthien-5-yl)-2,1,3-benzothiadiazole]-2′,2″-diyl) (F8TBT) and poly(9,9-dioctylfluorene-co-benzothiadiazole) (F8BT). In blends with F8TBT, P3HT is found to reorganize at low annealing temperatures (100 °C or below), evidenced by a red-shift of both absorption and photoluminescence (PL), and by a decrease in PL lifetime. Annealing to 140 °C, however, is found to optimize device performance, accompanied by an increase in PL efficiency and lifetime. Grazing incidence small angle X-ray scattering (GISAXS) is also performed to study the evolution in film nanomorphology with annealing, with the 140 °C-annealed film showing enhanced phase separation. We conclude that

reorganization of P3HT alone is not sufficient to optimize device performance but must also be accompanied by a coarsening of the morphology to promote charge separation. We also study the shape of the photocurrent action spectra of P3HT:F8TBT devices, aided by optical modeling of the absorption spectrum of the blend in a device structure. We observe changes in the shape of the photocurrent action spectra with annealing, and these are attributed to changes in the relative contribution of each polymer to photocurrent as morphology and polymer conformation evolve. In particular, in as-spun films from xylene, photocurrent is preferentially generated from ordered P3HT segments attributed to the increased charge separation efficiency in ordered P3HT compared to disordered P3HT. For optimized devices, photocurrent is efficiently generated from both P3HT and F8TBT. In contrast to blends with F8TBT, P3HT is only found to reorganize in blends with F8BT at annealing temperatures of over 200 °C. The low efficiency of the P3HT:F8BT system can then be attributed to poor charge generation and separation efficiencies that result from the failure of P3HT to reorganize.

Keywords: Polymer solar cells, polymer blends, organic photovoltaic devices, charge generation, energy transfer, GISAXS

1. Introduction

Solution-processed polymer solar cells are a promising new class of photovoltaic technology.[1] The ability to efficiently deposit thin films over large areas at low cost may provide polymer solar cells with an edge over rival technologies. However, while device performance has been steadily improving over the last 10 years, with polymer/fullerene blends recently demonstrating power conversion efficiencies over 5 %,[2, 3] further improvements in efficiency are necessary for commercialization. We have recently

demonstrated power conversion efficiencies of nearly 2 % for devices based on blends of the donor poly(3-hexylthiophene) (P3HT) with the acceptor poly((9,9-dioctylfluorene)-2,7-diyl-alt-[4,7-bis(3-hexylthien-5-yl)-2,1,3-benzothiadiazole]-2′,2′′-diyl) (F8TBT).[4] Other research groups have achieved similar efficiencies with different polymer/polymer combinations.[5, 6] These results indicate that competitive efficiencies may also be gained with all-polymer blends. The success of the P3HT:F8TBT system in particular may be attributed to the high charge carrier mobility of the P3HT phase that promotes efficient charge separation,[7] overcoming the problem of geminate recombination that has plagued many all-polymer blends.[8] Indeed, the higher fill factor and larger optimum film thickness can both be attributed to the reduction in required electric field strength to separate electron-hole pairs localized at blend interfaces.[9] Similar to P3HT/fullerene blends,[10] annealing is required to optimize device performance. In a previous study, we have investigated the influence of annealing on device operation, demonstrating that annealing induces an ordering of the P3HT phase that produces an order of magnitude increase in hole mobility.[7] From investigation of the electric field and light intensity dependence of photocurrent it was concluded that the improvement in efficiency with annealing originates from an increase in the separation efficiency of geminate electron-hole pairs with increased hole mobility and phase separation. In this paper we investigate the photophysics associated with charge generation (that is, exciton dissociation) and separation in P3HT:F8TBT blends. Due to the complex photophysics of P3HT, in particular the strong influence of intermolecular coupling on absorption and emission,[11] subtle yet significant changes in the photophysics of the blend with annealing are seen that are associated with the evolution of morphology and polymer conformation. These changes are used to help explain the variation in device performance with annealing, in particular the properties of films in optimized devices. These photophysical studies are further aided by a grazing incidence small angle X-ray scattering

(GISAXS) study of film nanomorphology, photocurrent action spectroscopy and optical modeling. Finally, we also compare the photophysics of P3HT:F8TBT blends with that of P3HT:poly(9,9-dioctylfluorene-co-benzothiadiazole) (F8BT) blends and discuss the origin of the lower efficiency of the P3HT:F8BT system.[12]

2. Results and Discussion

2.1. Photophysics of P3HT:F8TBT films

Figure 1 presents the chemical structures, HOMO/LUMO levels and optical absorption and photoluminescence spectra of regioregular P3HT, and F8TBT. While P3HT and F8TBT have similar band gaps, P3HT exhibits a broader absorption spectrum with prominent vibronic features. These vibronic peaks in P3HT films are not present in the optical absorption spectrum of P3HT in solution, and have been attributed to weakly interacting H-aggregates in ordered regions of the P3HT film where the polymer forms lamellar structures.[13] Indeed, the strength of the shoulder at ~ 600 nm has been related to the degree of interchain order in regioregular P3HT and may be used as a probe of film microstructure.[14] P3HT films also exhibit a larger extinction coefficient than films of F8TBT, with the absorption spectra in figure 1 normalized to film thickness. Comparing the photoluminescence (PL) of these two materials, F8TBT is more luminescent, with a photoluminescence quantum efficiency (PLQE) of 35% compared to only 4% for P3HT. The PL of P3HT also exhibits vibronic peaks associated with intermolecular coupling. In comparison, P3HT in solution and regiorandom P3HT films show featureless, blue-shifted PL spectra. The low PLQE of regioregular P3HT films is something of a mystery, with P3HT in solution exhibiting a PLQE of ~ 30 %[15] and regiorandom films a PLQE of 10 – 15 %. While this low PLQE is related to the increase in interchain coupling in regioregular P3HT

films, the exact mechanism is not clear, having been attributed to interchain dimer formation[16] and polaron generation.[15]

Figure 2 presents the absorption and emission spectra of P3HT:F8TBT blends spin-coated from xylene as a function of annealing temperature. The weight ratio for all studies was 1:1 P3HT:F8TBT by weight, and the annealing time was fixed at 10 minutes for all samples. The absorption spectrum of the as-spun film shows a lower absorption coefficient and less structure at 520 nm, 550 nm and 600 nm where ordered P3HT exhibits vibronic peaks. Additionally, the as-spun film shows a higher absorption coefficient at lower wavelengths that can be attributed to blue-shifted absorption by disordered or "solution-like" P3HT. With annealing, the absorption at these lower wavelengths is diminished, consistent with the ordering of P3HT. Examining the change in the absorption spectra with annealing at the 600 nm vibronic peak (see also figure 2(c)), an annealing temperature of only 100 °C is sufficient to produce an apparent full ordering of P3HT. X-ray diffraction studies of thick P3HT:F8TBT blends also show an increase in peak height and narrowing of the width of the (100) peak with annealing at 100 °C.[17] Above an annealing temperature of 140 °C the absorption intensity decreases, for reasons which are unclear at present.

The evolution of the emission spectra with annealing, figure 2 (b), shows an initial red-shift and decrease in intensity with annealing, with the emission spectrum then blue-shifting and increasing in intensity with annealing above 120 °C (see also the plot of PLQE vs annealing temperature in figure 2 (c)). We attribute the red-shift and decrease in PL intensity in the blend with annealing at 100 °C to the reorganization of P3HT chains that is observed in absorption spectroscopy. Indeed, a vibronic peak at 725 nm can be distinguished in the PL spectra of the 100 °C-annealed film that matches the peak seen in pristine P3HT films. The fact that P3HT vibronic structure can be observed in the PL spectrum of the 100 °C-annealed film also indicates that the majority of emission is originating from ordered

P3HT, consistent with our previous analysis of PL spectra.[7] With annealing above 120 °C, PL increases in intensity with a peak emerging at 700 nm that matches the emission peak of F8TBT. The emergence of F8TBT emission can be attributed to increased F8TBT domain size and / or purity, due to a coarsening of the blend, with fewer F8TBT excitons reaching an F8TBT/P3HT interface and recombining radiatively. Therefore it appears that reorganization of P3HT occurs at temperatures lower than that required for significant phase-separation. This is consistent with previous observations in P3HT:PCBM blends where an initial improvement in device performance with annealing is seen for temperatures of ~ 50 °C that has been linked to P3HT reorganization.[18] Only with annealing above the glass transition temperature of F8TBT (~ 100 °C) does F8TBT emission begin to dominate over P3HT emission. Interestingly, although the PLQE of the blend monotonically increases with annealing above 120 °C, at the highest annealing temperature (200 °C) the PLQE still remains relatively low (< 4 %) compared to the PLQE of F8TBT (35 %). This observation suggests that at these high annealing temperatures either the size of the F8TBT domains are not much larger than the exciton diffusion length, or that there is still a small minority P3HT component in the F8TBT phase acting as quenching sites.

The photoluminescence decay profiles of as-spun and annealed P3HT:F8TBT films (**figure 3** with lifetimes tabulated in **table 1**) are also consistent with this interpretation. The decay of as-spun films is slower than pure P3HT films, consistent with emission from disordered P3HT chains. With mild annealing, the photoluminescence decay quickens with the ordering of the P3HT phase. At higher anneal temperatures, the decay then becomes slower as a result of the increased emission from F8TBT that has a longer lifetime. The lack of a long-lived, red-shifted emission also suggests that exciplex formation is not energetically favorable in this blend combination.

2.2 GISAXS data

To support our photophysical and device data (section 2.3 below) we have also preformed grazing incidence small angle X-ray scattering (GISAXS) to provide independent morphological information. GISAXS is a powerful advanced scattering technique that allows the internal nanostructure of thin polymer films to be probed.[19] Previous X-ray photoelectron spectroscopy (XPS) investigations of P3HT:F8TBT films have provided evidence of vertical stratification in the form of P3HT-rich capping and wetting layers.[7] Thus while previous atomic force microscopy (AFM) investigations of as-spun and 140 °C-annealed P3HT:F8TBT films revealed little change in surface topography,[7] these measurements probe only the surface layer of the blend and are insensitive to bulk structure.

Figure 4 presents 2d GISAXS scattering patterns of as-spun, 100 °C-annealed, 140 °C-annealed and 180 °C-annealed P3HT:F8TBT films. These 2d scattering patterns provide information about lateral film structure as well as vertical film structure. From the evolution of the 2d pattern qualitative structural changes can be determined. The vertical diffuse scattering (q_z) shows a special type of oscillation due to correlated roughness. This modulation found in the vertical direction is an indication of the formation of a layered structure, consistent with our previous XPS observations of P3HT-rich capping and wetting layers. The horizontal scattering signal (q_y) provides information about the evolution of the lateral structure with annealing. With increasing anneal temperature the 2d scattering pattern becomes narrower which is direct evidence of a coarsening of structures in the plane of the film. For further analysis horizontal cuts were taken at the critical angle of the polymers (figure 4(b)). Fitting of the data (see experimental section) exhibits a structure size in the range of several hundreds of nanometres which is independent of the annealing temperature. Nevertheless the width, i.e. polydispersity, of this structure decreases which corresponds to an increased dominance of larger structure. Furthermore, a second smaller length scale

evolves with temperature, consistent with a hierarchy of phase separation that has been observed for nanostructured PFB:F8BT blends.[20] Whereas for the as-spun film no additional finer length-scale could be detected, the film annealed at 100 °C reveals a structure size in the range of 25 nm. For higher annealing temperatures this structure coarsens to ~ 100 nm for an annealing temperature of 140 °C and to ~ 150 nm for an annealing temperature of 180 °C. Thus although in the optical absorption spectra we saw a plateau in the degree of P3HT order at 100 °C, the GISAXS data provides direct evidence for a continuing evolution of the morphology at higher anneal temperatures consistent with the observed increase in PLQE with annealing. It should be noted that the structure sizes obtained via this fitting represent distances between objects in the film (eg domains), rather than the size of the domains themselves. Although we observe quite a large characteristic length-scale for the 140 °C-annealed film, the film structure may consist of smaller, pure P3HT domains laterally separated in an enclosing, impure F8TBT phase. Indeed, the relatively large characteristic length-scale observed in the 180 °C–annealed sample suggests that low PLQE in this and the 200 °C-annealed film is due to a residual minority component of P3HT that still serves to efficiently dissociate excitons. More complex modeling of the GISAXS data will be performed to reveal further quantitative information about the structure of these films.

2.3 Device characteristics of P3HT:F8TBT solar cells

Figure 5 examines the device characteristics of P3HT:F8TBT solar cells based on films prepared identically to those for the photophysical studies. The current-voltage characteristics of cells tested under simulated sunlight (figure 5 (a)) show that device performance improves with post-fabrication annealing up to an optimal annealing temperature between 130 °C and 140 °C. Open-circuit voltage also varies with annealing temperature, increasing systematically from 0.69 V for as-spun films to 0.98 V for an

annealing temperature of 200 °C. (We note that the insertion of a thin layer of LiF between the top of the blend film and the aluminum electrode improves the open-circuit voltage to 1.15 V independent of anneal temperature, comparable to the open-circuit voltages reported in with our previous publication that employed a higher molecular weight F8TBT yet exhibited high open-circuit voltages without the need for LiF. We attribute the lower open-circuit voltage of the devices here to the significantly higher dark currents, with LiF acting as a hole-blocking layer. See supporting information for dark current-voltage characteristics.) The spectral dependence of external quantum efficiency of P3HT:F8TBT devices measured under lower light intensities is plotted in figure 5(b) and also shows an optimal annealing temperature of 140 °C. Comparing the device and photophysical measurements (see figure 2 (c)) and in light of the above discussion, the device characteristics are interpreted as follows. Given that P3HT reorganizes at 100 °C yet device performance peaks at 140 °C, reordering of P3HT alone is evidently not sufficient to optimize device performance. Indeed, it is apparent that additional coarsening of the morphology evidenced by the GISAXS data above and the increase in F8TBT emission is required to promote device action. This observation is similar to the recent work of Chiu et al. who studied P3HT:PCBM blends and have shown that in addition to the growth of P3HT crystals that occurs with annealing at 100°C, higher annealing temperatures are required to grow the size of the PCBM domains in order to fully optimize device performance.[21] The existence of an optimum domain size stems from the need to balance the two processes of charge generation (exciton diffusion and dissociation at interfaces) and charge separation (separation of geminate electron-hole pairs localized at the donor-acceptor interface).[8] Thus while an intimately mixed morphology benefits exciton dissociation, a phase separated morphology benefits the separation of coulombically bound charge pairs at the donor-acceptor interface.

2.4 Photocurrent spectroscopy and optical modeling

Comparing now the shape of the photocurrent action spectra of as-spun and 140 °C-annealed devices (normalized in **figure 6**(a)), the as-spun device appears to exhibit a stronger response at the 600 nm P3HT shoulder. That is, despite the increase in absorption at the 600 nm shoulder in P3HT:F8TBT films with annealing, when compared as normalized curves the optimized 140 °C-annealed film shows a relative decrease in photocurrent at 600 nm compared to the as-spun film. This suggests on first glance that the increase in absorption at 600 nm as P3HT reorganizes is not realized as additional photocurrent. In other words, excitons generated in ordered P3HT segments appear not to be efficiently harvested in P3HT:F8TBT blends. However, the data of figure 6(a) may be misleading as there is a net increase in photocurrent at 600 nm with annealing (EQE increases from 3 % to 11 %) with figure 6(a) comparing only relative spectral changes. A better assessment of the efficiency of charge generation at a particular wavelength is facilitated by optical modeling of the absorption in the active layer. With knowledge of the optical constants of various layers in the device (glass, ITO, PEDOT:PSS, P3HT:F8TBT blend and Al electrode) it is possible to calculate the absorptance of the active layer (i.e. the fraction of incident photons absorbed by the active layer), allowing a direct comparison of the shape of the photocurrent action spectra to shape of the relevant absorption spectrum. The active layer was considered as a homogenous layer with the optical constants (*n* and *k*) of the blend determined with a spectroscopic ellipsometer and numerical fitting. The optical absorption spectrum of the blend film was calculated using *n* and *k* determined in this fashion and found to match perfectly the optical absorption spectrum measured using an absorption spectrometer. With knowledge of *n* and *k* of the active layer (and the optical constants of the other layers taken from the literature) the absorptance of the active layer in the full device configuration was calculated using an optical model that accounts for the transmission and reflection of all

layers.[22] Full details of the ellipsometry and optical modeling can be found in the supporting information. **Figure 7** compares the photocurrent action spectra of as-spun and annealed films to the calculated active layer absorptance spectra. Examining the results of the annealed film first, figure 7(b), there is actually a good agreement between the shape of the absorptance spectrum and the photocurrent action spectrum, suggesting a near uniform internal quantum efficiency at all wavelengths. In contrast, the as-spun film shows an enhancement in photocurrent relative to the film absorptance at long wavelengths. We understand the apparent enhanced photocurrent generation at long wavelengths as follows. Although the majority of P3HT in the as-spun xylene blend is disordered, there is a minority component that is ordered, confirmed by the smaller, but still discernable shoulder at 600 nm in the absorption spectrum of the as-spun blend. As geminate recombination has been shown to be the limiting mechanism in these devices, particularly under lower light intensities,[7] photoexcitation of ordered P3HT segments is more likely to result in separated charges (and hence photocurrent) compared to photoexcitation of disordered P3HT as the higher local hole mobility in ordered P3HT segments aids charge separation.[23] Therefore the photoexcitation of the minority component of ordered P3HT regions that provides a high charge separation efficiency accounts for a more than representative contribution to photocurrent at these wavelengths. The reason for the relative decrease in photocurrent at 600 nm with annealing most likely results from the increase in the size of P3HT domains, with fewer P3HT excitons reaching a donor-acceptor interface compared to F8TBT excitons. Thus the variation in the shape of the photocurrent action spectra in xylene-processed films reflects the variation in the relative contribution of F8TBT and P3HT to device action.

Additional supporting evidence for this interpretation is provided by examining films processed from chloroform. Due to the low boiling point of chloroform and chloroform being a good solvent for both polymers, as-spun films from chloroform are close to the one-phase

or intermixed region of the phase-diagram. This intimate mixing is confirmed by absorption spectroscopy, with the as-spun film exhibiting a broad, featureless absorption spectrum lacking vibronic structure; and by device measurements with as-spun chloroform films exhibiting EQEs of less than 1 % (see supporting information for photophysical and device measurements of chloroform-processed films). Annealing of chloroform-processed films dramatically improves device performance, with EQEs of 20 % demonstrated for films annealed at 140 °C (see supporting information) resulting from an ordering of P3HT and coarsening of morphology.[7, 8] Therefore the absence of ordered P3HT in as-spun chloroform films facilitates a clearer distinction when comparing the photocurrent action spectra of as-spun and annealed films. Comparing now the normalized photocurrent spectra of as-spun and annealed chloroform films (figure 6(b)) it is clear that a photocurrent shoulder at 600 nm exists in the annealed film that is absent in the as-spun film, confirming that photocurrent is produced from absorption at this low energy shoulder characteristic of ordered P3HT.

2.5 P3HT:F8BT blends

Finally, we examine the photophysics of blends of P3HT with the polyfluorene copolymer F8BT. F8BT is chemically similar to F8TBT (see **figure 8** for structure and energy levels) yet is found to be much less efficient in blends with P3HT.[12] A previous study has attributed the low efficiency of P3HT:F8BT devices to the low electron mobility in F8BT relative to PCBM.[12] However, F8BT is measured to have an electron mobility of ~ 10^{-3} cm^2 V^{-1} s^{-1} by the time-of-flight method[12] compared to an electron mobility of only ~ 10^{-5} cm^2 V^{-1} s^{-1} measured for F8TBT in blends with P3HT.[24] An order of magnitude lower electron mobility for F8TBT compared to F8BT is also calculated from transistor characteristics.[25] Given that P3HT:F8TBT blends can achieve reasonable efficiencies

despite the relatively poor electron mobility of F8TBT, the origin of the poor efficiency of P3HT:F8BT blends is worth reexamining.

Figure 9 presents the device characteristics of 1:1 P3HT:F8BT blends. Similar to P3HT:F8TBT blends, an increase in device performance for P3HT:F8BT blends is seen with annealing, with peak EQE increasing from 1 % for as-spun films to 6 % for films annealed at 100 °C, some 4 times higher than the best efficiencies obtained by Kim et al. who examined only as-spun films.[12] Higher annealing temperatures, however, are found to reduce device performance. Except for the device annealed at 220 °C, the current-voltage characteristics of P3HT:F8BT devices show very poor fill factors, symptomatic of poor charge separation efficiency, figure 9(a). Examining the absorption spectra of P3HT:F8BT blends as a function of annealing, **figure 10**(a), anneal temperatures of over 200 °C are required to facilitate the reorganization of P3HT (for reference, the T_g of F8BT is 140 °C[26]). Furthermore, at these high annealing temperatures the morphology of the blend is compromised, with AFM images revealing micron-sized features and large surface roughness (see supporting information). Thus unlike P3HT:F8TBT blends where P3HT is observed to reorganize at low annealing temperatures, the interaction of F8BT with P3HT in solid-state blends appears to hinder P3HT crystallization. Further evidence for the reorganization of P3HT with annealing above 200 °C is seen in the current-voltage curve of the 220 °C-annealed device. In particular, the fill factor improves substantially, and the current under forward bias increases dramatically indicative of a large increase in carrier mobility. However, due to the severe phase separation that occurs at this high anneal temperature, device efficiency is severely affected. The origin of this interaction is not fully understood at present. Comparison of the solubility parameters of P3HT (6.4 (cal cm^{-3})$^{1/2}$)[27], F8BT (10.0 (cal cm^{-3})$^{1/2}$)[28] and F8TBT (10.4 (cal cm^{-3})$^{1/2}$) for the similar APFO-3[28] that does not have alkyl groups on the thiophene units) suggests that

the interaction parameter for P3HT/F8BT and P3HT/F8TBT will be similar and unlikely to easily account for the differences seen here.

The PL spectra of P3HT:F8BT blends are shown in figure 10(b). While there appears to be good quenching of F8BT emission, there is residual emission characteristic of disordered P3HT. Indeed, a PLQE of 8 % is measured for the as-spun blend compared to 56 % for F8BT and ~ 4 % for P3HT. Photoluminescence excitation spectroscopy measurements (see supporting information) reveal that there is efficient energy transfer of F8BT excitons to the lower band-gap P3HT due to the good overlap between the emission of F8BT and the absorption of P3HT, consistent with the previous report of efficient red LEDs based on P3HT:F8BT blends.[29] Thus energy transfer from emissive F8BT to P3HT gives the appearance of good photoluminescence quenching, however the residual P3HT emission suggests that even charge transfer may not be as efficient as in P3HT/F8TBT blends. The PL spectrum of the P3HT:F8BT blend does not change significantly with annealing over the temperature range of 100 to 160 °C, and no F8BT emission is observed until the blend is annealed above 200 °C. Therefore issues associated with efficient charge generation *and* charge separation in this system resulting from the failure of P3HT to reorganize at low annealing temperatures appear to account for the inefficient operation of the P3HT:F8BT system rather than poor charge transport. Thus while the individual and complementary properties of P3HT and F8BT, namely their high charge transport mobilities, overlapping absorption spectra and offset energy levels, make them appear ideal as a photovoltaic combination, their unfavorable mixing properties prevent this realization.

3. Conclusions

We have studied the photophysics and photocurrent generation mechanisms in blends of P3HT with the polyfluorene co-polymers F8TBT and F8BT. In blends with F8TBT, P3HT

reorganizes at an annealing temperature of 100 °C evidenced by a red-shifting of the absorption spectrum and decrease in PLQE and PL lifetime. Reorganization of P3HT alone is not sufficient for optimum device performance, with higher anneal temperatures required that coarsen phase separation (as evidenced by GISAXS) promoting charge separation. An annealing temperature of 140 °C is found to be optimum that balances the processes of charge generation and charge separation. From photocurrent spectroscopy studies aided by optical modeling, photocurrent is efficiently generated from both polymers in the blend, with changes in the shape of the photocurrent action spectra with annealing resulting from changes in the relative contribution of each polymer to photocurrent due to the different onset temperatures of P3HT reorganization and bulk phase-separation. In blends with F8BT, P3HT was observed to reorganize only at annealing temperatures above 200 °C. The failure of P3HT to reorganize at low annealing temperatures in P3HT:F8BT blends explains the lower photovoltaic performance of this blend.

4. Experimental

F8TBT and F8BT were supplied by Cambridge Display Technology Ltd. with molecular weights (M_w) of 54 kg mol^{-1} and 150 kg mol^{-1} respectively. P3HT was supplied by Merck with molecular weight 26 kg mol^{-1} and a regioregularity of 94 %. Blend solutions were prepared with a weight ratio of 1:1 P3HT:F8TBT or P3HT:F8BT from either anhydrous xylene (Romil; mixed isomers) or chloroform (Romil) and spin-coated onto either quartz (Spectrosil B) for optical measurements, silicon wafer (with native oxide) for GISAXS measurements, or PEDOT:PSS-coated indium-tin oxide substrates for device fabrication with thickness of 70 - 80 nm. All solutions were heated at 70 °C for several hours to ensure that both polymers were fully dissolved. Films spin-coated from chloroform were spin-coated at room-temperature, whereas films spin-coated from xylene were spin-coated from a hot

solution to prevent P3HT precipitation. Devices were completed by evaporation of 100 nm of aluminum deposited at a vacuum of better than 10^{-6} mbar. Annealing of films was performed in a nitrogen glove box with devices annealed after cathode deposition. Samples were placed onto the hotplate preheated to the desired temperature, left for a fixed annealing time of 10 minutes and then quenched to room temperature. Devices were encapsulated after annealing but prior to removal from the glove box and testing.

Device external quantum efficiency (EQE) was evaluated as a function of wavelength at intensities of $\leq$ 0.1 mW cm^{-2}, with short-circuit current recorded using a Keithley 237 source measure unit (SMU). Current-voltage characteristics were acquired under simulated sunlight (100 mW cm^{-2} air mass (AM) 1.5 global spectrum) from an Oriel 81160-1000 solar simulator calibrated to a silicon reference cell. The spectral mismatch was calculated to be 0.80.

Absorption spectra were acquired using a Hewlett Packard 8453 diode array spectrometer. PL spectra and efficiencies were measured at room temperature in a nitrogen-purged integrating sphere with excitation from an argon ion laser at 488 nm and detection with an Oriel Instaspec IV spectrometer. PL efficiencies were calculated as described by de Mello et al. [30] Time-correlated single photon counting (TCPSC) data were obtained using a 470 nm diode laser (PicoQuant LDH 400) with a 80 ps full width at half-maximum at a 10 MHz repetition rate. PL was detected with a microchannel plate photomultiplier tube (Hamamatsu Photonics) coupled to TCSPC electronics (Lifespec-ps and VTC900 PC card, Edinburgh Instruments).

Grazing incidence small angle X-ray scattering (GISAXS) experiments were performed at the beamline BW4 of the DORIS III storage ring at HASYLAB (DESY, Hamburg) [19]. To allow penetration of the X-ray beam inside the polymer film an incident angle of α_i = 0.52° which is well above the critical angles of the polymers was chosen,

ensuring that the entire volume of the whole film was probed. The sample detector distance was set to 2.04 m and the wavelength to $\lambda = 0.138$ nm. With this experimental setting lateral structure sizes from 4 nm up to 1 μm are resolved. Two beam stops blocked the direct beam as well as the strong specular reflection. The scattering signal was recorded with a two-dimensional detector (MARCCD). To achieve lateral structural information of the scattering pattern, horizontal cuts were conducted which were fitted with a mathematical model including a resolution function and two structural contributions. Specifically, the horizontal cuts were fitted in the effective surface approximation of the distorted wave Born approximation (DWBA) [31] by assuming polydisperse objects with well defined nearest neighbour distances d_1 and a possible domain structure d_2. Both characteristic structural lengths d_1 and d_2 were assumed to follow a Lorentzian distribution with a width s_1 and s_2. Taking the experimental resolution function into account the parameters d_1, d_2, s_1 and s_2 were fitted.

Ellipsometry measurements were made using a J.A. Woollam M-2000 diode-array rotating compensator ellipsometer with a xenon light source, over wavelength range of 300 – 850 nm, and fitted with the WVASE32 software to determine *n* and *k*. Measurement was made of films of 70 – 80 nm thickness on quartz substrates. Full details of the fitting procedures and optical modeling can be found in the supporting information.

Received: ((will be filled in by the editorial staff))
Revised: ((will be filled in by the editorial staff))
Published online: ((will be filled in by the editorial staff))

[1] A. Mayer, S. R. Scully, B. E. Hardin, M. W. Rowell, M. D. McGehee, *Materials Today* **2007**, *10*, 28

[2] J. Y. Kim, K. Lee, N. E. Coates, D. Moses, T. Q. Nguyen, M. Dante, A. J. Heeger, *Science* **2007**, *317*, 222.

[3] J. Peet, J. Y. Kim, N. E. Coates, W. L. Ma, D. Moses, A. J. Heeger, G. C. Bazan, *Nat. Mater.* **2007**, *6*, 497.

[4] C. R. McNeill, A. Abrusci, J. Zaumseil, R. Wilson, M. J. McKiernan, J. J. M. Halls, N. C. Greenham, R. H. Friend, *Appl. Phys. Lett.* **2007**, *90*, 193506.

[5] T. Kietzke, H.-H. Hörhold, D. Neher, *Chem. Mater.* **2005**, *17*, 6532.

[6] S. C. Veenstra, J. Loos, J. M. Kroon, *Prog. Photovolt: Res. Appl.* **2007**, *15*, 727.

[7] C. R. McNeill, J. J. M. Halls, R. Wilson, G. L. Whiting, S. Berkebile, M. G. Ramsey, R. H. Friend, N. C. Greenham, *Adv. Funct. Mater.* **2008**, *18*, 2309

[8] C. R. McNeill, S. Westenhoff, C. Groves, R. H. Friend, N. C. Greenham, *J. Phys. Chem. C* **2007**, *111*, 19153

[9] P. Peumans, S. R. Forrest, *Chem. Phys. Lett.* **2004**, *398*, 27.

[10] V. D. Mihailetchi, H. Xie, B. de Boer, L. J. A. Koster, P. W. M. Blom, *Adv. Funct. Mater.* **2006**, *16*, 699.

[11] P. J. Brown, D. S. Thomas, A. Köhler, J. S. Wilson, J.-S. Kim, C. M. Ramsdale, H. Sirringhaus, R. H. Friend, *Phys. Rev. B.* **2003**, *67*, 064203.

[12] Y. Kim, S. Cook, S. A. Choulis, J. Nelson, J. R. Durrant, D. D. C. Bradley, *Chem. Mater.* **2004**, *16*, 4812.

[13] J. Clark, C. Silva, R. H. Friend, F. Spano, *Phys. Rev. Lett.* **2007**, *98*, 206406.

[14] J. F. Chang, J. Clark, N. Zhao, H. Sirringhaus, D. W. Breiby, J. W. Andreasen, M. M. Nielsen, M. Giles, M. Heeney, I. McCulloch, *Phys. Rev. B.* **2006**, *74*, 115318.

[15] S. Cook, A. Furube, R. Katoh, *Energy Environ. Sci.* **2008**, *1*, 294

[16] I. F. Perepichka, D. F. Perepichka, H. Meng, F. Wudl, *Adv. Mater.* **2005**, *17*, 2281

[17] H.-G. Flesch, R. Resel, C. R. McNeill, *Organic Electronics* **2009**, Submitted.

[18] W. Ma, C. Yang, X. Gong, K. Lee, A. J. Heeger, *Adv. Funct. Mater.* **2005**, *15*, 1617.

[19] P. Müller-Buschbaum, *Anal. Bioanal. Chem.* **2003**, *376*, 3

[20] C. R. McNeill, B. Watts, S. Swaraj, H. Ade, L. Thomsen, W. J. Belcher, P. C. Dastoor, *Nanotechnology* **2008**, *19*, 424015.

[21] M. Y. Chiu, U. S. Jeng, C. H. Su, K. S. Liang, K. H. Wei, *Adv. Mater.* **2008**, *20*, 2573.

[22] N. K. Persson, H. Arwin, O. Inganas, *J. Appl. Phys.* **2005**, *97*.

[23] R. A. Marsh, C. Groves, N. C. Greenham, *J. Appl. Phys.* **2007**, *101*, 083509.

[24] C. R. McNeill, N. C. Greenham, *Appl. Phys. Lett.* **2008**, *93*, 203310.

[25] J. Zaumseil, C. R. McNeill, M. Bird, D. L. Smith, P. P. Ruden, M. Roberts, M. J. McKiernan, R. H. Friend, H. Sirringhaus, *J. Appl. Phys.* **2008**, *103*, 064517.

[26] C. L. Donley, J. Zaumseil, J. W. Andreasen, M. M. Nielsen, H. Sirringhaus, R. H. Friend, J. S. Kim, *J. Am. Chem. Soc.* **2005**, *127*, 12890.

[27] J. Jaczewska, I. Raptis, A. Budkowski, D. Goustouridis, J. Raczkowska, M. Sanopoulou, E. Pamula, A. Bernasik, J. Rysz, *Synth. Met.* **2007**, *157*, 726

[28] S. Nilsson, A. Bernasik, A. Budkowski, E. Moons, *Macromolecules* **2007**, *40*, 8291

[29] Y. Kim, D. D. C. Bradley, *Curr. Appl. Phys.* **2005**, *5*, 222

[30] J. C. de Mello, H. F. Wittmann, R. H. Friend, *Adv. Mater.* **1997**, *9*, 230.

[31] P. Müller-Buschbaum, in *Applications of Synchrotron Light to Scattering and Diffraction in Materials and Life Sciences*, Vol. 776 (Eds: T. A. Ezquerra, M. Garcia-Gutierrez, A. Nogales, M. Gomez), Springer, Berlin **2009**, 61

Figure 1. (a) Chemical structures and energy level diagrams of P3HT and F8TBT. (b) Absorption and photoluminescence spectra of P3HT (solid) and F8TBT (dashed) films processed from xylene.

Figure 2. Evolution of the photophysical properties of xylene-processed P3HT:F8TBT films with annealing. (a) Absorption spectra, (b) photoluminescence spectra, (c) PLQE. Part (c) also plots the strength of the absorption at 600 nm as a function of annealing and the short-circuit current of P3HT:F8TBT devices under solar illumination extracted from figure 5.

Figure 3. Photoluminescence decay profiles of as-spun and annealed P3HT:F8TBT blend films processed from xylene. Also shown for comparison are the decay kinetics of pure P3HT and F8TBT films.

Figure 4. (a) 2d GISAXS scattering pattern of as-spun and annealed (100 °C , 140 °C and 180 °C) P3HT:F8TBT films. The colour code represents the scattering intensity. The specular reflection is shielded by a beam stop. (b) Double logarithmic plot of the out-of-plane cuts of the GISAXS data taken at the critical q-value of F8TBT (q_z=0.52 nm^{-1}). The data (black triangles) are fitted (red solid lines) with a mathematical model. The dashed line represents the resolution limit. All curves are shifted along the y-axis for clarity.

Figure 5. Variation in the device characteristics of xylene-processed P3HT:F8TBT photovoltaic devices with annealing. (a) Current voltage characteristics under simulated sunlight (100 mW cm^{-2} AM1.5G), (b) Spectral dependence of external quantum efficiency.

Figure 6. Normalized plots of external quantum efficiency vs. wavelength comparing the shape of as-spun and annealed films for processed from (a) xylene and (b) chloroform.

Figure 7. Comparison of the shape of photocurrent action spectra (squares) to the simulated device optical absorption spectra (solid line) for (a) as-spun and (b) annealed devices.

Figure 8. Energy level diagrams, chemical structures, absorption and photoluminescence spectra of F8BT and P3HT films.

Figure 9. Device characteristics of P3HT:F8BT blends as a function of annealing routine. (a) Current voltage characteristics under simulated sunlight (100 mW cm^{-2} AM1.5G), (b) photocurrent action spectra.

Figure 10. Photophysical properties of P3HT:F8BT blends. (a) Absorption spectra, (b) photoluminescence spectra.

Table 1. Summary of photoluminescence decay lifetimes obtain from a biexponential fit (~ $a_1\exp(-t/\tau_1) + a_2\exp(t/\tau_2)$) to the data of figure 3.

	α_1	τ_1 [ns]	α_2	τ_2 [ns]
F8TBT	1	2.35	-	-
P3HT	0.68	0.21	0.42	0.49
As-spun	0.81	0.64	0.24	2.40
140°C	0.93	0.50	0.18	1.48
180°C	0.85	0.78	0.18	2.08

The interplay between polymer order, phase separation (see figure) and photovoltaic efficiency in blends of poly(3-hexylthiophene) (P3HT) with polylfluorene copolymers is investigated. The choice of polyfluorene copolymer is shown to influence the temperature at which P3HT orders in the blend and hence the device efficiency achievable. In addition to ordered P3HT phases, a degree of phase separation is also required to facilitate charge separation.

Keyword: Photovoltaic Devices

Dr. C. R. McNeill, A. Abrusci, I. Hwang, M. A. Ruderer, Prof. Dr. P. Müller-Buschbaum, Dr. N. C. Greenham

Photophysics and photocurrent generation in polythiophene/polyfluorene co-polymer blends

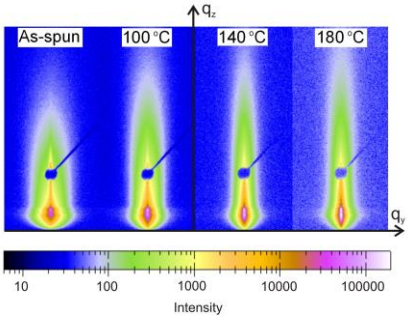

Column Title: *C. R. McNeill et al.*/Photocurrent generation in polythiophene/polyfluorene blends